ChemPubSoc Europe

DOI: 10.1002/celc.201902115

CHEMELECTROCHEM Articles

# Improvement of Oxygen-Depolarized Cathodes in Highly Alkaline Media by Electrospinning of Poly(vinylidene fluoride) Barrier Layers

Marcus Gebhard,*[a] Tim Tichter,[b] David Franzen,[c] Melanie C. Paulisch,[d] Konstantin Schutjajew,[e] Thomas Turek,[c] Ingo Manke,[d] and Christina Roth[a]

Oxygen-depolarized cathodes (ODC) were developed for chlor-alkali electrolysis to replace the hydrogen evolution reaction (HER) by the oxygen reduction reaction (ORR) providing electrical energy savings up to 30% under industrially relevant conditions. These electrodes consist of micro sized silver grains and polytetrafluoroethylene, forming a homogeneous electrode structure. In this work, we report on the modification of ODCs by implementing an electrospun layer of hydrophobic poly (vinylidene fluoride) (PVDF) into the ODC structure, leading to a significantly enhanced ORR performance. The modified electrodes are physically characterized by liquid flow porometry, contact angle measurements and scanning electron microscopy. Electrochemical characterization is performed by linear sweep voltammetry and chronopotentiometry. The overpotential for ORR at application near conditions could be reduced by up to 75 mV at 4 kA m$^{-2}$ and 135 mV at a higher current density of 9.5 kA m$^{-2}$. Consequently, we propose that modifying ODCs by electrospinning is an effective and cost-efficient way to further reduce the energy demand of the ORR in highly alkaline media.

## 1 Introduction

Industrial processes, such as the chlor-alkali electrolysis,[1–5] demand large quantities of energy. Between 2,200–2,600 kWh are consumed per ton of chlorine in a conventional membrane NaCl electrolysis process.[6,7] This high energy demand is in turn responsible for a major share of $CO_2$ emissions. In order to reduce the electrical energy demand of the chlor-alkali electrolysis process and thus the corresponding $CO_2$ emissions, significant progress has been made by replacing the so far used hydrogen-evolving cathodes[8–12] by oxygen depolarized cathodes (ODC).[13–19] In this manner electric energy savings of up to 30% can be achieved under industrially relevant conditions (80–90 °C, 30 wt.% NaOH electrolyte).[20] Since the oxygen reduction reaction (ORR) has a higher standard electrode potential compared to the hydrogen evolution reaction (HER) [Eqs. (1) and (2)] the overall cell potential can be lowered to approx. 2 V resulting in savings of up to 1 V.

$$\text{HER}: \ 2\,H_2O + 2\,e^- \rightarrow H_2 + 2\,OH^- \qquad E^0 = 0.00\,\text{V (vs. RHE)} \tag{1}$$

$$\text{ORR}: \ 2\,H_2O + O_2 + 4\,e^- \rightarrow 4\,OH^- \qquad E^0 = 1.23\,\text{V (vs. RHE)} \tag{2}$$

State-of-the-art ORR catalysts are carbon supported, platinum based materials providing excellent activity and stability in acidic media.[21–26] However, regarding the harsh conditions during technical electrolysis, carbon-based materials have been proven to be insufficiently stable due to carbon corrosion. Hence, commercial ODC for chlor-alkali electrolysis are carbon-free materials. Since silver provides an oxygen reduction activity similar to platinum under strongly alkaline conditions[27,28] it has been chosen to be a suitable substitute for platinum. In this context, studies of Moussallem et al.[29] focused on variations of silver precursors and compositions of silver-based GDE and lead to optimized electrodes regarding energy consumption and long-term stability. Herein, micro sized silver powder is mixed with PTFE as binder and methylcellulose in an aqueous solution, spray coated on a nickel mesh, hot pressed and sintered to form the porous gas diffusion electrode. Even though, ODCs perform well in industrial scale application, it is necessary to further improve their performance. Improvements of existing electrodes are based on an increase of the three-phase boundary providing an enhanced catalyst utilization.[30] How-

[a] M. Gebhard, Prof. C. Roth
Electrochemical Process Engineering
University of Bayreuth
Universitätsstraße 30, 95447 Bayreuth, Germany
E-mail: marcus.gebhard@uni-bayreuth.de
[b] T. Tichter
Institute of Chemistry and Biochemistry
Freie Universität Berlin
Takustraße 3, 14195 Berlin, Germany
[c] D. Franzen, Prof. T. Turek
Institute of Chemical and Electrochemical Process Engineering
Clausthal University of Technology
Leibnizstrasse 17, 38678 Clausthal-Zellerfeld, Germany
[d] Dr. M. C. Paulisch, Dr. I. Manke
Institute of Applied Materials
Helmholtz-Zentrum Berlin für Materialien und Energie GmbH
Hahn-Meitner-Platz 1, Berlin 14109, Germany
[e] K. Schutjajew
Institute of Chemistry, University of Potsdam
Karl-Liebknecht-Str. 24–25, 14476 Potsdam, Germany



 

ever, tuning the three-phase boundary is not a straightforward task since the electrolyte distribution inside the porous structure remains unknown. To overcome this issue Paulisch et al.[31] investigated the electrolyte invasion and distribution during operation in a first approach, using X-ray computed tomography. The results revealed a potential dependent electrolyte transport through the ODC as well as a droplet formation on its gas side. Nevertheless, further research with in-situ imaging techniques has to be done to precisely correlate structure properties and electrochemical performance, as it is crucial to identify the electrolyte distribution inside the porous structure and the corresponding limitations.

However, without knowing the bottle neck of the electrode performance it is difficult to predict how existing electrodes can be further improved. Two main approaches to overcome this issue are: a) empirical and systematic studies as well as b) modeling approaches. Regarding a) Franzen et al.[32] investigated the influence of PTFE binder content on the electrode performance and changed systematically the silver to binder ratio. However, no significant effect compared to the state of the art ODCs could be observed. Regarding b) a dynamic one-dimensional three-phase model was published by Röhe et al.[33] Besides a description of the gas-liquid equilibrium, the model considers the activities of the species in the reaction kinetics, which is essential due to the high electrolyte concentrations. As a result, Röhe et al. identified the following mechanism: The ORR leads to an enrichment of hydroxide ions close to the gas-liquid interface, which in turn causes a lowering of the water activity. The lowered water activity, in turn, decreases the oxygen solubility, which will limit the current density. Based on these findings, the authors draw the conclusion that a high electrode performance requires a good mass transport of water and hydroxide ions in the liquid phase as well as an extended gas-liquid interface. The strong influence of water and ion transport on the performance of the electrodes was also confirmed experimentally.[34] As a consequence, it is essential to achieve an optimized electrolyte boundary e. g. by a variation of the hydrophobic part of the GDE. In fact, various studies report on the change in hydrophobicity by different techniques, such as a) variation of polymer coating and content,[35–37] b) fluorination[38] and c) laser irradiation[39] of the GDEs. However, since these reports refer to fuel cell related applications only, the results can not necessarily be transferred to ODCs.

In this work, we suggest to locally increase the hydrophobicity of the ODC by implementing a thin layer of PVDF into the conventional Ag and PTFE electrode structure, instead of an overall variation of the hydrophobic content in the electrode. For this purpose we utilize the electrospinning technique since it is a versatile tool to form porous and tailored polymer fiber structures.[40–42] Furthermore, previous publications successfully applied electrospinning of PVDF for the preparation of hydrophobic fiber materials for various applications.[43–47] Since electrospinning is a low cost method, which is easily scalable for industrial production,[48–50] we consider it as a promising and feasible way to incorporate additional highly hydrophobic layers in ODCs to modify the electrolyte distribution.

The modified electrodes are investigated and compared to unmodified electrodes by physical methods like scanning electron microscopy (SEM), contact angle determination (CA), electrical conductivity, real density and porometry measurements as well as BET surface area measurements. Furthermore the electrodes' ORR performance is investigated using an in-house built electrochemical half-cell set-up. The comparison to conventionally prepared ODCs with polarization curves and stability tests for 10 hours at different loads shows the superior performance of our electrospun modified ODCs.

## Experimental Section

### Electrode preparation

ODCs were fabricated by a combination of an airbrushing process similar to Ref.[29] and an electrospinning step. At first an aqueous suspension of micro sized silver catalyst (SF9ED, Ferro, Germany) and PTFE (PTFE Dispersion TF 5060GZ, 3 M Dyneon, Germany) were mixed with a methylcellulose solution (WALOCELMKX 70000 PP 01) using an Ultra-Turrax (IKA®-Werke GmbH & CO. KG, Germany). 20 layers of this suspension were consecutively air brushed (Evolution, 0.6 mm pin hole, Harder & Steenbeck, Germany) onto each side of a conductive supporting material (Ni-mesh 106 μm × 118 μm mesh size, 63 μm thickness, Haver & Boecker OHG, Germany).

Subsequently, the electrospinning of PVDF was performed at room temperature and a relative humidity $<40\,\%$ utilizing an electrospinning set-up from IME Technologies (DG_V1_100-EC-DG, Waalre, Netherlands). The electrospinning solution was prepared by adding 16 wt.% poly(vinylidene fluoride) PVDF (Sigma Aldrich, Mw ~534.000 g $mol^{-1}$) to a mixture (1 : 1 w/w) of acetone (>99,5 %, Sigma Aldrich) and N,N-dimethylacetamide DMAc (>99 %, Carl Roth). The solution was stirred at 70 °C for 24 h prior to electrospinning and subsequently transferred to a syringe, connected by PTFE tubing to a needle (Ø = 0.4 mm). Previously prepared ODCs were mounted on the fiber collector of the electrospinning device to apply a thin layer of PVDF. Electrospinning was performed for 5 min to one side of the electrode only (Figure 1) at a voltage of 12–15 kV and a distance of 30 cm between the nozzle and the fiber collector using a flow rate of 10 μl $min^{-1}$.

Finally, the spraying process of the silver-PTFE suspension was continued on both sides of the electrode for additional 20 layers. Resulting electrodes were further processed in a hot-pressing step with a pressing load of 15 MPa at 130 °C for 5 min and a sintering step at 330 °C for 15 min to burn off the methylcellulose and improve the mechanical stability.

### Physical characterization

The hydrophobicity of the electrodes was evaluated by the determination of contact angles with deionized water (drop shape analyzing system DSA10, Krüss GmbH, Hamburg, Germany). The electrical conductivity was examined using an Agilent 34461 A Digital Multimeter in 4-point-sense mode. The real density was determined with a helium pycnometer (Pycnomatic ATC, Quantachrome). Flow-through pores and bubble point pressure were determined using capillary flow porometry (Porometer 3G, Quantachrome). The high-resolution images of the surface of the electrodes (Figure 2) were recorded by scanning electron microscopy using a REM Hitachi SU8030 (at 15.0 kV). BET surface areas were determined with krypton as probe gas using a 3 Flex

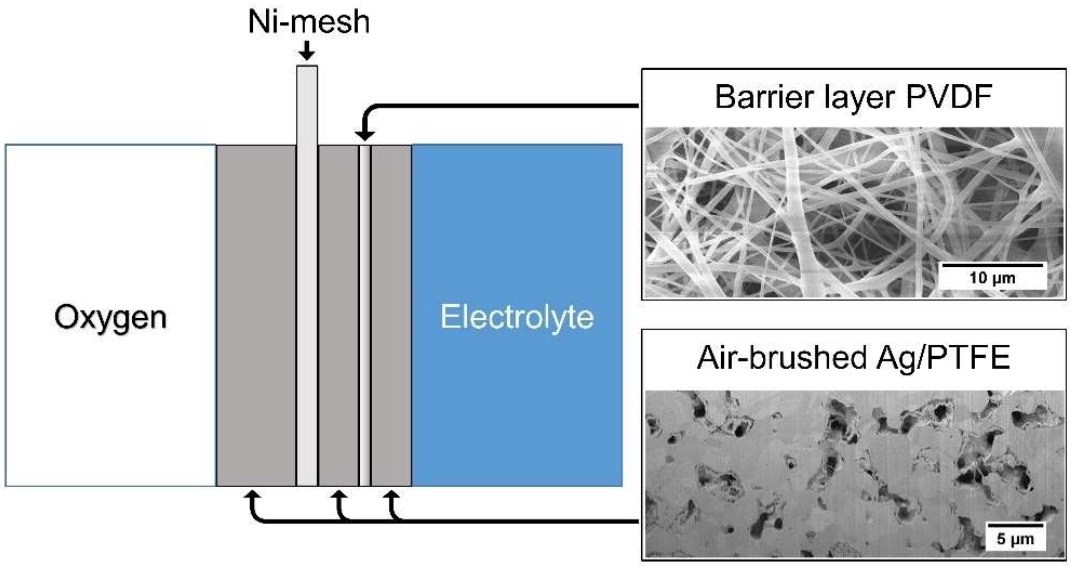


**Figure 1.** Schematic representation of the chosen orientation of the ODC and the corresponding position of the electrospun PVDF layer.

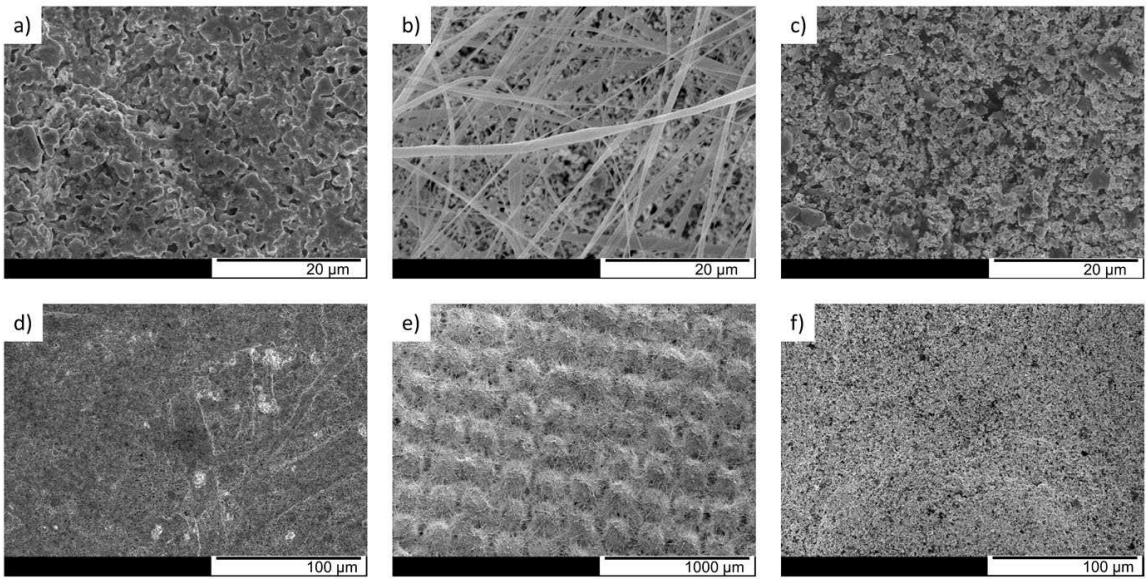


**Figure 2.** High-resolution SEM images of the modified ODC structure at different preparation stages, a/d) after initial spray deposition, b/e) after consecutive electrospinning process, c/f) after final spray deposition, hot-pressing and sintering process.

instrument (Micromeritics Instrument Corp.). To analyze the pore system in more detail, a high spatial resolution of the microstructure was obtained via scanning electron microscopy (SEM) and focused ion beam (FIB) technology using a Zeiss Crossbeam 340 Gallium-FIB/SEM (Oberkochen, Germany). For the coarse cut, 30 keV and 15 nA were applied and 30 keV and 7 nA for the polishing step.

### Electrochemical characterization

Electrochemical characterization of the ODCs was performed in a three-electrode set-up using an in house developed operando cell as presented in our previous publication[51] (2nd Gen. cell) using a Gamry Ref 3000 potentiostat (Gamry Instruments, USA). The gas side and the electrolyte containing side are separated by the ODC (Figure 1) which served as working electrode with a geometric surface area of 3.14 $cm^2$. In case of the modified ODC the barrier layer was placed towards the electrolyte as depicted in Figure 1. The choice of orientation for the symmetric conventional ODC is obsolete. A platinum wire electrode (99.95%, ø = 1 mm, l = 25 cm) served as counter electrode (CE). A HydroFlex® (Gaskatel GmbH, Germany) reversible hydrogen electrode (RHE) represented the reference electrode (RE). The electrolyte (30 wt.% NaOH solution) was prepared from caustic flakes (> 99% NaOH, Carl Roth, Germany) and deionized water (Merck Millipore, USA). On the backside of the ODC, dry oxygen (≥ 99.5%; Air Liquide, France) was supplied via a pressure controller (Everwand Druckgastechnik GmbH, Germany) by constant flow of 25 ml $min^{-1}$ (Influx Measurements Ltd, UK) and minimal backpressure using a 5 mm water column.

Modified and conventional ODCs were characterized at 80 °C operating temperature following the same sequence of electrochemical methods. At first a start-up procedure consisting of four successive chronopotentiometric steps (1; 2; 3; 4 kA m$^{-2}$, 15 min each) followed by a cell resistance determination using potentiostatic electrochemical impedance spectroscopy (1 MHz to 100 mHz, AC amplitude of 5 mV) was performed. The equilibrium potential of the ORR vs. RHE was determined to be 1.13 V using the calculations described by Franzen et al.[32] Subsequently, linear sweep voltammetry (LSV) measurements were conducted between the open circuit potential and a lower potential, limited by the devices current limitation of 3 A, at a potential sweep rate of 2 mV s$^{-1}$ using current interrupt (CI) mode for inner resistance (*iR*) correction. Finally, stability tests were performed at a chronopotentiometric load of 2; 4; 6; 4; 2 kA m$^{-2}$ for 2 h, respectively.

## 2 Results and Discussion

### 2.1. Electrode Preparation and Characterization

The modified ODCs were characterized at three steps during the preparation process to analyze the electrode properties prior and after the electrospinning process. The first state shows the ODC before electrospinning, the second immediately after electrospinning and the final third state after the sintering process. In Figure 2 a) and d) SEM images of the non-treated ODC (after the first steps of air-brushing) are shown in different magnifications. It can be seen that already at this stage the preparation provides a porous structure. The silver grains appear to be coated and connected with a homogenous film. This can be attributed to the methylcellulose and binder content of the spraying dispersion. Figure 2 b) and e) depict the electrode, coated with the hydrophobic PVDF fibers after the electrospinning step. It can be seen that the fibers form a highly porous structure that covers the surface homogeneously, despite that the underlying structure was dominated by the mesh structure of the nickel current collector. Individual fiber sizes range from 0.3 μm to 2 μm in diameter. Behind this fibrous layer, the underlying silver structure as depicted in Figure 2 a) and d) can still be seen. This suggests that the electrospun layer is sufficiently thin, so that the additional layers of silver, introduced by the subsequent air-brushing step will be in contact with the previous silver-layers and the electron conduction is not significantly disturbed. SEM images of the final surface structure after spraying, hot pressing and sintering are shown in Figure 2 c) and f). Here, the surface reveals a smooth and porous silver structure without the film observed in Figure 2 a) and d). Instead, small silver grains form the electrode surface.

Corresponding to the three preparation steps shown in Figure 2, contact angle measurements were performed at each stage to monitor the surface hydrophobicity. Figure 3 a) reveals the strong hydrophilic nature of the electrode after the first sprayed silver-PTFE layers. The hydrophilic methylcellulose dominates the properties and turns the so far unfinished electrode hydrophilic. Time dependent measurements in Figure 3 d) show an initial contact angle of 90° that decreases within 2 min to 45° since the water gets drawn towards the electrode. Contrarily, the electrospun PVDF renders the surface highly hydrophobic as seen in Figure 3 b). Even though the layer is porous and very thin, the sessile droplet does not

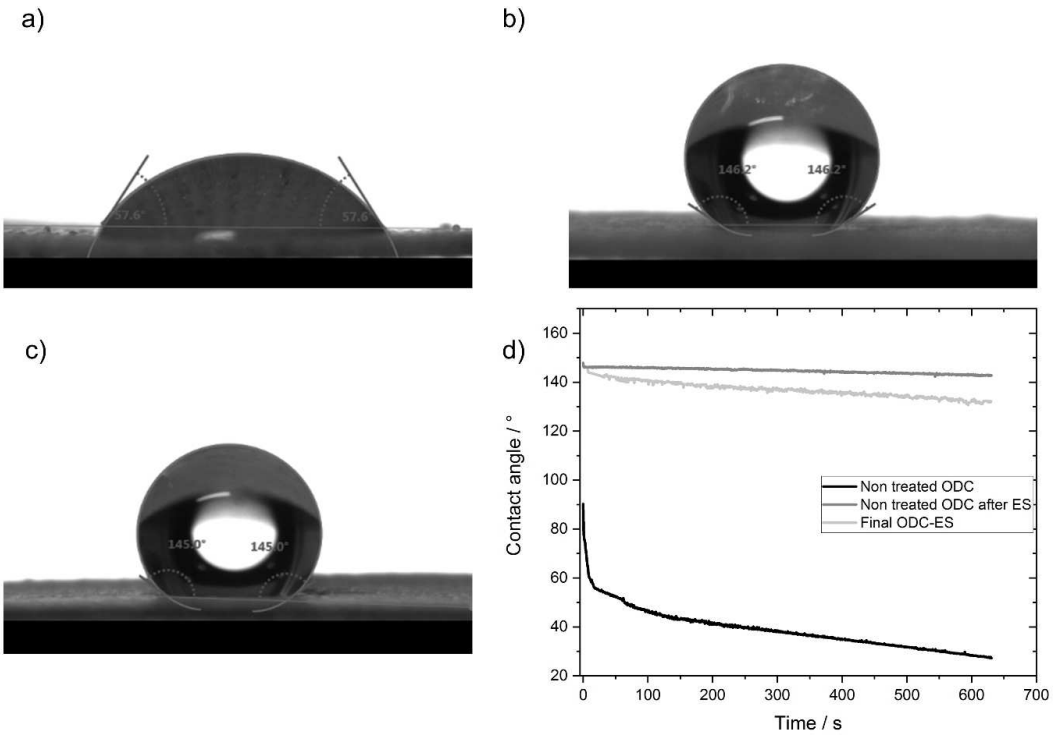


**Figure 3.** Contact angle measurements of the modified ODC structure at different preparation stages, a) after initial spray deposition, b) after consecutive electrospinning process, c) after final spray deposition, hot-pressing and sintering process, d) time dependent CA development.

interact with the underlying hydrophilic phase. An initial contact angle of 146° can be observed that remains unchanged over the whole measurement. These results clearly demonstrate that it was possible to apply a thin and hydrophobic layer by electrospinning PVDF onto the electrode. Further contact angle measurements were performed at the ODC surface after final spraying, pressing and sintering. The initial contact angle of 144° decreased within 2 min to 140°. Consequently, the surface can be considered slightly less hydrophobic when compared to the electrospun layer. The hydrophobic character of the surface can be attributed to the PTFE from the spraying dispersion that remained in the structure after sintering.

This surface is similar to an ODC without the electrospun PVDF layer. However, the composition and structure of the ODCs' surface assures that electrolyte intrusion into the pores is lowered, yet still possible to a certain degree.

Additional physical characterization with real density, with BET surface area measurements and with electrical conductivity tests does not provide any differences between the conventional and modified electrode. However, capillary flow porometry reveals a narrower pore size distribution and a small shift in minimal pore diameter for the modified electrode (Figure 4 a). The pore size distribution was also shifted to minimally lower values. While the bubble point and maximum remained nearly unchanged, the mean pore size is affected by the modification. The main difference between the samples was detected in the minimum pore size range. A fraction of the existing pores is obviously narrowed at their smallest diameter by the electrospinning process as shown in Figure 4 b). This could be explained by the additional polymer material which is partially blocking the pores after sintering.

To identify the location of the applied hydrophobic layer, FIB/SEM measurements were performed. Figure 5 depicts the internal structure of a conventional ODC in comparison to a modified ODC. While the conventional ODC shows a uniform structure through the whole electrode thickness (in agreement with the results of Franzen et. al),[31,32] the modified electrode reveals a comparably large pore system at approx. 50 µm from the ODC surface. The pore system spreads parallel to the electrode surface at the position where the electrospun PVDF is located. This increased pore system is most likely formed by the electrospun layer of fibrous PVDF during the hot pressing and sintering step.

Taking into account the physical characterization we conclude that the overall electrode structure was not substantially changed. Only a minor shift in the minimum pore diameter and the introduction of an additional pore system could be detected via liquid flow porometry and FIB/SEM.

### 2.2. Electrochemical Characterization

Based on the findings of Röhe et al.[33] the orientation of the modified ODC (electrospun PVDF layer facing towards the liquid electrolyte) was chosen as pointed out in the experimental section. In this manner the hydrophobic layer is supposed to act as a barrier that impedes major flooding of the electrode. Compared to the conventionally prepared electrode the electrolyte should therefore enter the modified electrode less far, and therefore shift the three-phase boundary towards the electrolyte bulk. Consequently, shorter transport pathways should lead to an increased performance as pointed out in Ref.[33].

For comparison of conventional ODCs to the modified ODCs, *iR* compensated polarization curves were recorded at application relevant conditions (80 °C, 30 wt.% NaOH). The polarization curves of the electrodes (Figure 6) reveal a clear trend of the electrochemical ORR performance. All electrodes provide nearly the same open circuit potential (1.10 V) and overpotential at low current densities. Differences are getting more pronounced at current densities beyond 0.5 kA m$^{-2}$ where the modified electrodes require significantly lower overpotentials for the ORR compared to the non-modified analogue. This trend reaches a maximum at the highest current density of 9.5 kA m$^{-2}$ (limited by the potentiostat). All four modified ODCs provide an improved ORR performance, despite their individual performance slightly deviates. At technically relevant conditions of 4 kA m$^{-2}$ the mean overpotential was lowered by approx. 60 mV, rendering them superior when compared to the non-modified electrode. At the highest tested current density of 9.5 kA m$^{-2}$ the average of modified ODCs provide an approx.

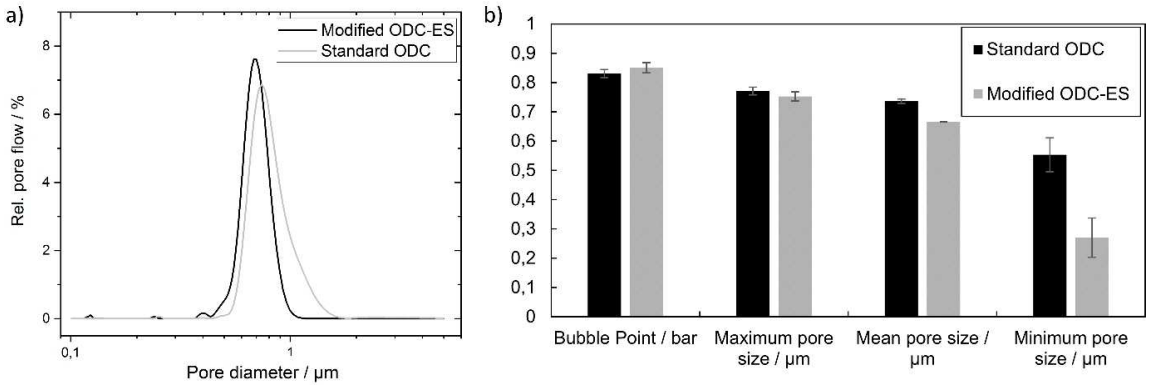


**Figure 4.** Evaluation of porometry measurements of modified ODC-ES with reference material 97 % Ag-3 % PTFE from, [32] a) comparison of pore size distribution, b) selected representative parameters.

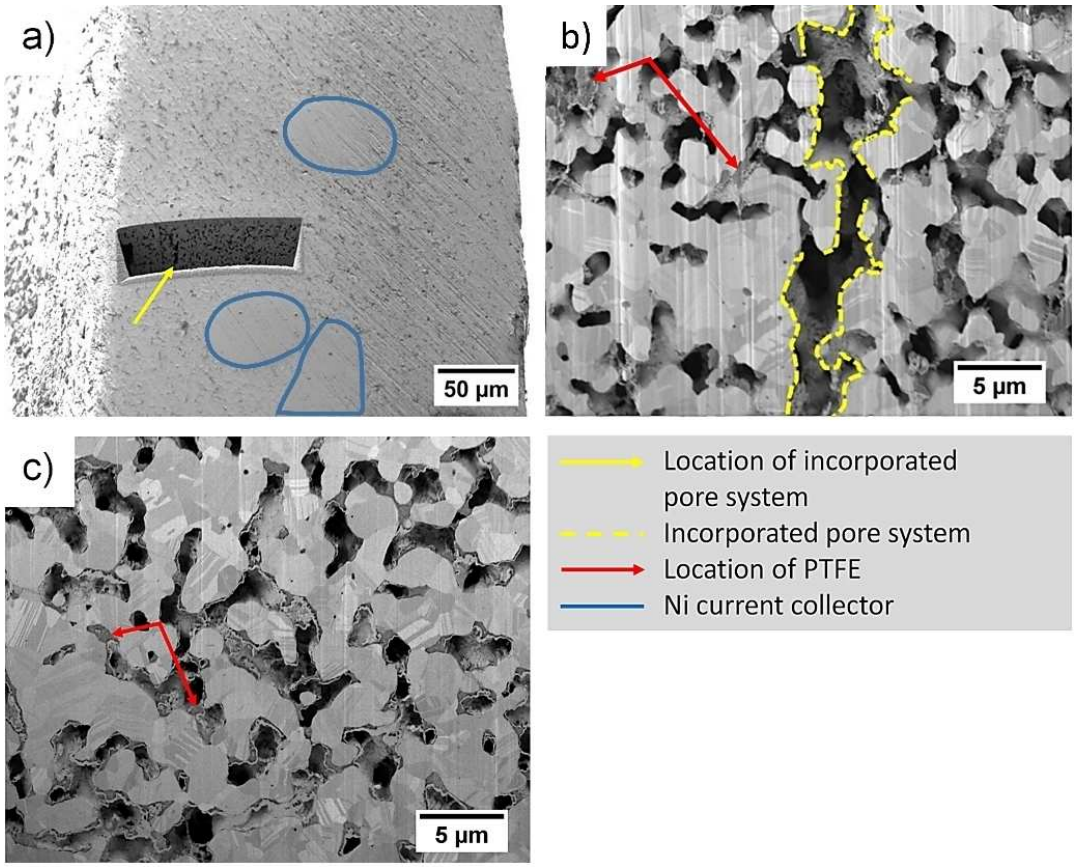


**Figure 5.** FIB/SEM images of a) cross section of the modified ODC-ES; location of the incorporated pore system, b) detail view of the microstructure near to the formal PVDF layer c) conventional ODC.

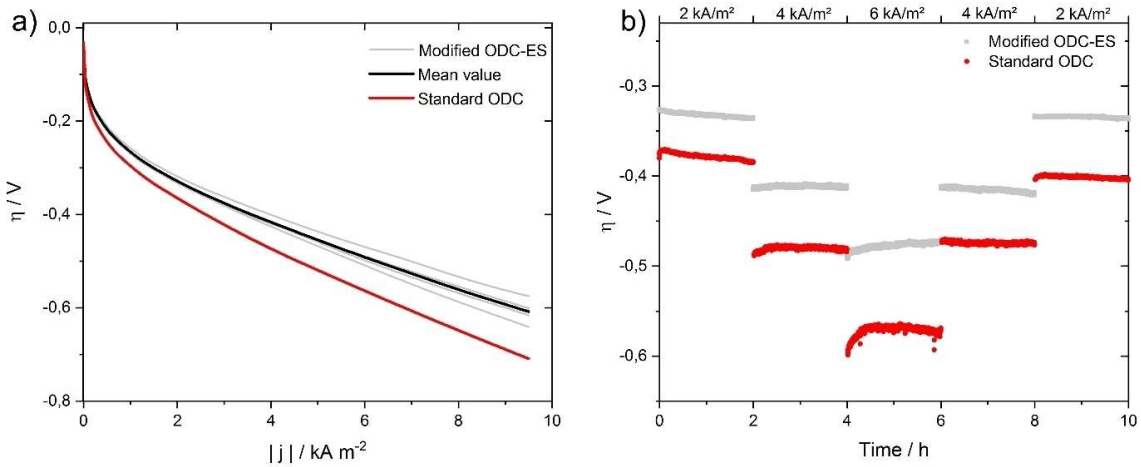


**Figure 6.** Electrochemical characterization of conventional ODC and modified ODC-ESs at 80 °C, 30 wt.% NaOH, a) polarization curves and b) chronopotentiometric measurements at different current densities.

100 mV lower overpotential for the ORR. It has to be noted that the best tested modified ODC outperforms the conventional ODC by 75 mV and 135 mV at 4 kA m$^{-2}$ and 9.5 kA m$^{-2}$, respectively. However, it is worth to mention that all electrodes, modified and non-modified, do not show any sign of mass transport limitations at high current densities.

As pointed out, a possible explanation for the improved ORR performance could be that the barrier layer impedes the electrolyte from flooding of pores beyond this point. The resulting shorter transport paths are one reasonable explanation for the improved performance of the modified ODC. However, since lower overpotentials could also be achieved by

an extension of the total three-phase boundary[33], the additional pore system (Figure 5 b) could also be responsible for the increased performance.

Additionally to the polarization curves shown in Figure 6 a), chronopotentiometric measurements were performed to demonstrate the durability of the enhanced ORR performance of the modified electrode. The experiments were carried out at application relevant conditions (80 °C and 30 wt.% NaOH) at different current densities over a period of 10 h. The current load was increased successively from 2 to 4 and 6 kA m$^{-2}$ for 2 h. It can be seen that both electrodes develop an increasing overpotential of about 10 mV during the first 2 h of operation and maintain their overpotential during the entire testing period at 4 kA m$^{-2}$. Nevertheless, the modified ODC performs at about 70 mV lower overpotentials compared to the non-modified ODC at 4 kA m$^{-2}$. These values are in good agreement with the results obtained from the polarization curves. At the highest current density of 6 kA m$^{-2}$ the modified ODC shows an overpotential of 85 mV that increases up to 95 mV suggesting that the performance increases with time, whereas the standard ODC shows constant overpotentials. During the ongoing current density steps to 4 kA m$^{-2}$ and 2 kA m$^{-2}$ both electrodes maintain a stable overpotential. It has to be mentioned that the modified ODC can be operated at 6 kA m$^{-2}$ at an overpotential where the conventional ODC is able to operate at the standard current density of 4 kA m$^{-2}$ only. Consequently, it can be concluded that the modified ODC maintains its improved performance and does not reveal any decay during a 10 hours testing period.

## 3. Conclusions

With this work, we report on a fabrication process of silver-based oxygen depolarized cathodes (ODCs) containing a hydrophobic layer of PVDF, introduced via electrospinning. It is demonstrated that significant improvement of the electrode performance regarding the oxygen reduction reaction can be achieved under highly alkaline conditions. The modified ODCs revealed overpotentials decreased by up to 75 mV at technically relevant current densities of 4 kA m$^{-2}$ compared to conventional ODCs. At higher current densities of 9.5 kA m$^{-2}$ potential saving up to 135 mV can be achieved. Chronopotentiometric measurements did not show any sign of performance loss over a 10 h testing period, underlining the stability of the electrodes at industrially relevant operating conditions. During the whole operating process the modified electrodes perform significantly better than their unmodified analogues. Consequently, we conclude that the modified electrodes are thus suited to further reduce the energy demand of the chlor-alkali electrolysis process.

## *Acknowledgments*

*Financial support for this study by Deutsche Forschungsgemeinschaft in the framework of the research unit "Multiscale analysis of complex three-phase systems: Oxygen reduction at gas-diffusion electrodes in aqueous electrolyte" (FOR 2397; research grants RO 2454/16-1, MA 5039/3-1 and TU 89/13-1) is gratefully acknowledged. We also want to thank the group of U. Krewer (TU Braunschweig) and M. Röhe. Open access funding is provided by the University of Bayreuth.*

**Keywords:** chlor-alkali electrolysis · electrospinning · gas diffusion electrode · oxygen-depolarized cathode · oxygen reduction reaction

[1] S. Lakshmanan, T. Murugesan, *Clean Techn. Environ. Policy* **2014**, *16*, 225.
[2] J. Crook, A. Mousavi, *Environ. Forensics* **2016**, *17*, 211.
[3] M. Grotheer, R. Alkire, R. Varjian, *Electrochem. Soc. Interface* **2006**, *15*, 52–54.
[4] P. Millet, *Chlor-alkali technology: fundamentals, processes and materials for diaphragms and membranes*, Woodhead Publishing, Cambridge, U. S. A., **2013**.
[5] T. F. O'Brien, T. V. Bommaraju, F. Hine, *Handbook of Chlor-Alkali Technology*, Springer US, Boston (MA), U. S. A., **2005**.
[6] J. Jörissen, T. Turek, R. Weber, *Chem. Unserer Zeit* **2011**, *45*, 172.
[7] D. Bergner, *J. Appl. Electrochem.* **1982**, *12*, 631.
[8] D. Brown, M. Mahmood, A. Turner, S. Hall, P. Fogarty, *Int. J. Hydrogen Energy* **1982**, *7*, 405.
[9] E. Endoh, H. Otouma, T. Morimoto, *Int. J. Hydrogen Energy* **1988**, *13*, 207.
[10] M. Gong, D. Y. Wang, C. C. Chen, B. J. Hwang, H. Dai, *Nano Res.* **2016**, *9*, 28.
[11] N. Yoshida, T. Morimoto, *Electrochim. Acta* **1994**, *39*, 1733.
[12] N. Yoshida, M. Yoshitake, E. Endoh, T. Morimoto, *Int. J. Hydrogen Energy* **1989**, *14*, 137.
[13] J. Moorhouse, *Modern Chlor-Alkali Technology, Volume 8*, John Wiley & Sons, New York, NY, **2008**.
[14] Y. Kiros, M. Pirjamali, M. Bursell, *Electrochim. Acta* **2006**, *51*, 3346.
[15] Y. Kiros, M. Bursell, *Int. J. Electrochem. Sci.* **2008**, *444*.
[16] J. Jung, S. Postels, A. Bardow, *J. Cleaner Prod.* **2014**, *80*, 46.
[17] T. Ashida, S. Wakita, M. Tanaka, Y. Nishiki, T. Shimamune, *Denki Kagaku* **1997**, *65*, 1026.
[18] J. Kintrup, M. Millaruelo, V. Trieu, A. Bulan, E. S. Mojica, *Electrochem. Soc. Interface* **2017**, *26*, 73.
[19] I. Moussallem, J. Jörissen, U. Kunz, S. Pinnow, T. Turek, *J. Appl. Electrochem.* **2008**, *38*, 1177.
[20] "Neues Verfahren senkt Energieverbrauch bei Chlor-Produktion um 30 %. Available online: https://www.process.vogel.de/neues-verfahren-senkt-energieverbrauch-bei-chlor-produktion-um-30-a-408117/14. Juni 2013 (accessed on 02.06.2016)".
[21] N. M. Marković, T. J. Schmidt, V. Stamenković, P. N. Ross, *Fuel Cells* **2001**, *1*, 105.
[22] Z. Qi, A. Kaufman, *J. Power Sources* **2003**, *113*, 37.
[23] C. Wang, N. M. Markovic, V. R. Stamenkovic, *ACS Catal.* **2012**, *2*, 891.
[24] J. Wu, H. Yang, *Acc. Chem. Res.* **2013**, *46*, 1848.
[25] C. Zhang, X. Shen, Y. Pan, Z. Peng, *Front. Energy* **2017**, *11*, 268.
[26] H. A. Gasteiger, S. S. Kocha, B. Sompalli, F. T. Wagner, *Appl. Catal. B* **2005**, *56*, 9.
[27] M. Chatenet, L. Genies-Bultel, M. Aurousseau, R. Durand, F. Andolfatto, *J. Appl. Electrochem.* **2002**, *32*, 1131.
[28] N. Furuya, H. Aikawa, *Electrochim. Acta* **2000**, 4251.
[29] I. Moussallem, S. Pinnow, N. Wagner, T. Turek, *Chem. Eng. Process.* **2012**, *52*, 125.
[30] P. Frania, *Dissertation*, Technische Universität Dortmund; Verlag Dr. Hut.
[31] M. C. Paulisch, M. Gebhard, D. Franzen, A. Hilger, M. Osenberg, N. Kardjilov, B. Ellendorff, T. Turek, C. Roth, I. Manke, *Materials* **2019**, *12*, *2686*.
[32] D. Franzen, B. Ellendorff, M. C. Paulisch, A. Hilger, M. Osenberg, I. Manke, T. Turek, *J. Appl. Electrochem.* **2019**, *49*, 705.
[33] M. Röhe, F. Kubannek, U. Krewer, *ChemSusChem* **2019**, *12*, 2373.
[34] M. Röhe, A. Botz, D. Franzen, F. Kubannek, B. Ellendorff, D. Öhl, W. Schuhmann, T. Turek, U. Krewer, *ChemElectroChem* **2019**, *6*, 5671.
[35] M. Lee, X. Huang, *Electrochem. Commun.* **2019**, *100*, 39–42.
[36] S. Park, B. N. Popov, *Fuel* **2009**, *88*, 2068–2073.

[37] R. Vijay, S. K. Seshadri, P. Haridoss, *Trans. Indian Inst. Met.* **2011**, *64*, 175–179.
[38] T. V. Nguyen, *J. Electrochem. Soc.* **2015**, *162*, F1451.
[39] M. Tomas, I. S. Biswas, P. Gazdzicki, L. Kullova, M. Schulze, *Mater. Renew. Sustain. Energy* **2017**, *6*, 20.
[40] S. Cavaliere, S. Subianto, I. Savych, D. J. Jones, J. Rozière, *Energy Environ. Sci.* **2011**, *4*, 4761.
[41] Z. M. Huang, Y. Z. Zhang, M. Kotaki, S. Ramakrishna, *Compos. Sci. Technol.* **2003**, *63*, 2223.
[42] D. H. Reneker, A. L. Yarin, *Polymer* **2008**, *49*, 2387.
[43] Z. Q. Dong, X. H. Ma, Z. L. Xu, W. T. You, F. B. Li, *Desalination* **2014**, *347*, 175.
[44] A. Razmjou, E. Arifin, G. Dong, J. Mansouri, V. Chen, *J. Membr. Sci.* **2012**, *415–416*, 850.
[45] L. Y. Wang, L. E. Yu, J. Y. Lai, T. S. Chung, *Sep. Purif. Technol.* **2018**, *205*, 184.
[46] L. Y. Wang, W. F. Yong, L. E. Yu, T. S. Chung, *J. Membr. Sci.* **2017**, *535*, 342.
[47] M. Tao, L. Xue, F. Liu, L. Jiang, *Adv. Mater.* **2014**, *26*, 2943.
[48] M. Yu, R. H. Dong, X. Yan, G. F. Yu, M. H. You, X. Ning, Y. Z. Long, *Macromol. Mater. Eng.* **2017**, *302*, 1700002.
[49] I. G. Kim, J. H. Lee, A. R. Unnithan, C. H. Park, C. S. Kim, *J. Ind. Eng. Chem. (Washington, D. C.)* **2015**, *31*, 251.
[50] X. Zhang, Y. Lu, *Polym. Rev.* **2014**, *54*, 677.
[51] M. Gebhard, M. Paulisch, A. Hilger, D. Franzen, B. Ellendorff, T. Turek, I. Manke, C. Roth, *Materials* **2019**, *12, 1275*.

Manuscript received: December 19, 2019
Revised manuscript received: January 24, 2020